

msb/cb 97- 206135

Final
IN-47-02
OIT
0945-8

Final Report
on

ANTHROPOGENIC SULFATE, CLOUDS, AND CLIMATE FORCING

NASA Contract NAGW-3735

**Steven J. Ghan
Atmospheric Sciences Group
Battelle Pacific Northwest Laboratory
Richland WA 99352**

submitted to

**Kenneth H. Bergman
Global Atmospheric Modeling and Analysis Program
Earth System Modeling and Global Analysis Branch
Code YSE
NASA Headquarters
Washington, DC 20546-0001**

February 21, 1997

1. Introduction

This research work is a joint effort between research groups at the Battelle Pacific Northwest Laboratory, Virginia Tech University, Georgia Institute of Technology, Brookhaven National Laboratory, and Texas A&M University. It has been jointly sponsored by the National Aeronautics and Space Administration, the U.S. Department of Energy, and the U.S. Environmental Protection Agency. In this research, a detailed tropospheric aerosol-chemistry model that predicts oxidant concentrations as well as concentrations of sulfur dioxide and sulfate aerosols has been coupled to a general circulation model that distinguishes between cloud water mass and cloud droplet number. The coupled model system has been first validated and then used to estimate the radiative impact of anthropogenic sulfur emissions.

Both the direct radiative impact of the aerosols and their indirect impact through their influence on cloud droplet number are represented by distinguishing between sulfuric acid vapor and fresh and aged sulfate aerosols, and by parameterizing cloud droplet nucleation in terms of vertical velocity and the number concentration of aged sulfur aerosols. Natural sulfate aerosols, dust, and carbonaceous and nitrate aerosols and their influence on the radiative impact of anthropogenic sulfate aerosols, through competition as cloud condensation nuclei, will also be simulated. Parallel simulations with and without anthropogenic sulfur emissions are performed for a global domain.

The objectives of the research are:

- To couple a state-of-the-art tropospheric aerosol-chemistry model with a global climate model.
- To use field and satellite measurements to evaluate the treatment of tropospheric chemistry and aerosol physics in the coupled model.
- To use the coupled model to simulate the radiative (and ultimately climatic) impacts of anthropogenic sulfur emissions.

These three objectives are addressed in sections 2, 3 and 4, respectively.

2. Model Development

During the period December 1995 – October 1996, good progress was made on several fronts in the effort to build the global aerosol model.

2.1 Aerosol properties

Proper treatment of direct and indirect radiative forcing by aerosols requires simulation of the aerosol physical size distribution, but most global chemistry models currently only simulate the aerosol mass concentration in the submicron size range. Direct radiative forcing is quite sensitive to particle size as the mass scattering efficiency peaks for particle sizes near the wavelength of light. Indirect forcing is sensitive to the number of particles active as CCN. Aerosol size distributions vary widely as aerosols are emitted as primary particles or nucleated as secondary particles, grow by condensation, are activated as CCN, processed by clouds, resuspended, and scavenged by precipitation. For example, activation of aerosol particles to form cloud droplets followed by precipitation scavenging of the cloud droplets can remove 85% of the aerosol mass but only 15% of the aerosol number. The particles that remain have a much smaller size. Such changes in size distribution cannot be simulated in models that only treat aerosol mass. Simulation of a wide range of particle sizes is therefore required.

Simulating the aerosol physical size distribution requires a numerical solution to the aerosol general dynamics equation (Friedlander, 1977). A number of solution techniques have been developed. The most direct technique involves discretization of the particle size range into a number of size bins and application of spline, sectional, or finite element solution techniques (Gelbard and Seinfeld, 1980). The number of prognostic aerosol fields with this approach is given by $N_{bins}N_{comp}$, where N_{bins} is the number of size bins or sections (typically 20 or more) and N_{comp} is the number of chemical components. In a 3-dimensional atmospheric model this becomes computationally burdensome.

The modal aerosol dynamics (MAD) approach (Giorgi, 1986; Whitby *et al.*, 1991) adopted for our model assumes that the aerosol population is composed of a set of log-normally distributed modes. The basis for this approach is that observed atmospheric aerosol size distributions are generally well characterized by the modal approach, and there is a theoretical basis for the existence of the different modes (Whitby 1978). Originally three size modes were used to characterize the atmospheric aerosol, but recent observations extending to sizes

below 10 nm diameter (Covert 1995) have shown the existence of four size modes: nuclei (sizes below 10 nm), Aitken (previously referred to as nuclei), accumulation, and coarse.

Each mode is described by three distribution parameters (number, geometric mean diameter, and geometric standard deviation), or equivalently, three moments of the mode's size distribution [e.g., number (0th moment), surface (2nd), and volume or mass (3rd)]. The evolution of the size distribution is described by equations for the three moments, and these equations include terms for emissions, new particle production, condensational growth, transport, etc. A simplification which we have adopted is to simulate number for each mode and mass for each component of each mode, and prescribe the geometric standard deviation. Aerosol components within each mode are assumed to be internally mixed, while different modes are assumed to be externally mixed. The resulting number of prognostic aerosol fields is then $N_{modes}(N_{comp}+1)$, where N_{modes} is the number of modes, which makes this method computationally more efficient than the sectional method.

Although we had originally planned to predict aerosol number as well as mass before the end of this project, we chose to devote more of our project resources toward the introduction of additional aerosol species and modes into the model. These additional species are needed to fully characterize the cloud condensation nuclei concentration. Currently the model treats sulfate, methanesulfonic acid (MSA), nitrate and carbonaceous aerosol in Aitken and accumulation size modes, and sulfate, soil dust and sea-salt in coarse size modes with prescribed size distributions. Although sulfate does not constitute a large mass fraction of the coarse modes, it can have a large effect on the cloud nucleating properties of predominantly dust particles because it is the only soluble component of the dust/sulfate mode. We have also begun to develop a treatment of biological aerosols, which may also be important as CCN (Jaenicke, 1993).

Carbonaceous (carbon containing) aerosols have two components: organic carbon (OC) aerosols which consist of organic compounds, and black carbon (BC) aerosols, also referred to as soot or elemental carbon, which are strongly light absorbing. Sources for carbonaceous aerosols are similar in magnitude to those for sulfate aerosol (Penner, 1995), as are aerosol mass concentrations (Malm *et al.*, 1994). Thus carbonaceous aerosols should be important in radiative forcing (Penner *et al.*, 1992). Compared to sulfate aerosols, carbonaceous aerosols are chemically much more complex, and their sources and atmospheric concentrations are

less well quantified.

The carbonaceous aerosols are treated as part of the Aitken and accumulation mode aerosols, internally-mixed with sulfate and nitrate. Primary carbonaceous aerosols in the coarse size range are generally negligible compared to soil dust and sea-salt and are ignored. The assumption of an internal mixture is not completely valid near source regions where BC aerosol particles can be initially distinct and also hydrophobic (Hallberg *et al.*, 1994). However, as the aerosols age through condensation and coagulation, the BC becomes more internally mixed. Also, BC aerosol sources are only about 10% of the total carbonaceous aerosol sources, so treating fresh BC aerosols as a distinct externally-mixed mode does not appear necessary. OC aerosols are partially water soluble, and their water uptake can be treated as in Malm *et al.* (1994). They also act as efficient CCN (Eagan *et al.* 1974, Novakov and Penner 1993). The appropriate treatment of mixed OC and sulfate particles in the aerosol activation module will require some experimentation however.

2.2 Emissions of primary aerosols

Primary aerosols are those emitted as particles. These include sea salt, soil dust, carbonaceous, and biological aerosols.

Sea-salt emissions are not specified directly. The sea-salt concentration at 10 m is prescribed as a function of windspeed (Erickson and Duce, 1988), and the net transfer (turbulent and gravitational settling) between this height and the model's lowest layer acts as a net source for sea-salt particles.

Soil dust emissions follow the parameterization of Gillette and Passi (1988). Emissions of dust are particularly sensitive to soil moisture and surface wind speed. We have found that the soil moisture and surface wind speed simulated at R15 resolution (the finest resolution affordable using the comprehensive chemistry mechanism) are not realistic enough to produce a realistic dust simulation. We have therefore resorted to using analyzed soil moisture and winds to drive the simulation. The soil moisture analysis is taken from the monthly mean NCEP/NCAR reanalysis (Kalnay *et al.*, 1996), which of course depends upon the particular surface hydrology model employed but is based on a much finer spatial resolution (T62) than R15. The winds in our simulation are nudged toward ECMWF twice-daily analysis, along with temperature and surface pressure, using Newtonian relaxation (Jeuken *et al.*, 1996).

The sum of OC and BC emissions from anthropogenic activities are taken from Liousse *et al.* (1994). The BC component due to fossil fuel is taken from Penner *et al.* (1993), and the BC component from biomass burning is estimated from estimates of CO₂ emissions and an assumed BC emission factor.

Emissions of biological aerosols are poorly known. We have surveyed the literature and found that outdoor bioaerosols are dominated by bacteria, pollens, and fungal spores, with most mass in the coarse mode. We are developing an initial treatment of bioaerosol emissions in which the local emission strength is a function of season and the surface vegetation, and the total emissions are calibrated by comparison of simulated and observed surface bioaerosol concentrations.

2.3 Emissions of aerosol precursors

Aerosol precursors are those gases that, after oxidation, condense to form aerosol particles. These include SO₂, DMS, NO_x, biogenic hydrocarbons, and non-methane hydrocarbons. In addition, emissions of those species that influence oxidant concentrations, such as CO, are also needed.

Most of the trace-gas global emissions inventories that are needed by the model have been obtained. Emissions from the Global Emissions Inventory Activity (GEIA) (Graedel, 1994) have been utilized whenever possible and will continue to be incorporated into our efforts as new data releases and species inventories become available. So far from the GEIA repository we are utilizing the SO₂ and NO_x inventories of Benkovitz *et al.* (1996) and the biogenic hydrocarbon inventory of Guenther *et al.* (1995). For other species, anthropogenic hydrocarbon emissions are taken from Piccot *et al.* (1992) and DMS emissions are taken from Spiro *et al.* (1992). CO emissions are calculated as in Easter *et al.* (1994) using emission factors applied to inventories of co-emitted species. Trace-gas emissions from biomass burning are obtained by applying emissions factors to the CO₂ inventory of Hao *et al.* (1990). Ammonia emissions are from Dentener and Crutzen (1994).

2.4 Oxidation of aerosol precursors

For oxidation of aerosol precursors, we have developed two mechanisms, one highly sim-

plified and the other more comprehensive. The simplified version focuses on the sulfur cycle, while the comprehensive version predicts organics and nitrogen oxides. The simple chemistry version is based on the CO-CH₄ mechanism used in Easter *et al.* (1994) and Saylor *et al.* (1996) and derived from the mechanism of Lelieveld and Crutzen (1990) with simple sulfur chemistry added. CO and H₂O₂ are treated as transported species, distributions of NO_x, O₃, and CH₄ are prescribed, and other non-sulfur species (primarily radicals) are calculated using a pseudo-steady-state approximation. Oxidant concentrations (OH, H₂O₂, and O₃) are then used to calculate the gas- and aqueous-phase oxidation of sulfur dioxide (SO₂) to sulfuric acid (H₂SO₄) and the gas-phase oxidation of dimethyl sulfide (DMS) to SO₂ and methanesulfonic acid (MSA). The yields of SO₂ and MSA from DMS oxidation are based on the work of Kreidenweis and Seinfeld (1988).

The simple chemistry mechanism is computationally very inexpensive but has a number of limitations. Its treatment of DMS oxidation is highly simplified, it does not treat the formation of nitrates, it prescribes ozone and nitrogen oxides, and most importantly, it does not treat non-methane hydrocarbons (NMHC), which strongly affect the oxidant concentrations (O, OH, H₂O₂).

With support from NASA and EPA, we therefore have developed a more detailed chemical mechanism that is still fast enough for global applications. It is based on the Carbon Bond Mechanism (CBM4) developed by Gery *et al.* (1989). The choice was based primarily on the compactness of the mechanism due to its lumped structure approach for the treatment of hydrocarbons. The structural-lumping technique categorizes the reactions of similar carbon bonds, thus requiring fewer surrogate species as opposed to the molecular-lumping approach used in the Regional Acid Deposition Model (RADM2) chemical mechanism developed by Stockwell *et al.* (1990). Although RADM2 has more hydrocarbon species and more comprehensive interactions of various intermediates and radicals that are either ignored or not retained in CBM4, they are of little value in this situation since the available global emission inventories are themselves poorly resolved among hydrocarbon species.

We have modified CBM4 for global chemical modeling by explicitly treating the lesser reactive paraffins such as methane and ethane, and their intermediates methyl and ethyl peroxy radicals. These modifications are similar to the treatment in RADM2. The modified CBM4 has 40 species and 92 reactions. It runs almost twice as fast as RADM2 and predicts

very similar sulfate and other trace species concentrations.

The simple chemistry mechanism simulates oxidant concentrations (OH, HO₂, H₂O₂, etc.) well under pristine conditions. However, the performance quickly deteriorates in the presence of NMHCs under moderately to even slightly polluted rural scenarios. The modified CBM4 predicts lower oxidant concentrations under polluted rural scenarios as compared to the simple mechanism which neglects NMHC reactions. Figure 1 shows overprediction of sulfate and nitrate by simple chemistry due to higher oxidant concentrations. The plot shows sulfate and nitrate concentrations after one day for different rural scenarios of slight to moderate pollution (NO_x ranged from 0.1-2.0 ppb and NMHC/NO_x ranged from 0.5-25ppb).

The simplified chemistry mechanism crudely distinguishes between sulfuric acid vapor, which can form new aerosol particles through homogeneous nucleation, and MSA, which cannot. To improve this partitioning, we have derived a condensed dimethyl sulfide (DMS) photo-oxidation mechanism from the comprehensive mechanism proposed by Yin *et al.* (1990) (which is comprised of 50 sulfur species and 166 sulfur reactions). The comprehensive scheme has been condensed by eliminating consistently unimportant reactions for several scenarios of varying NO_x, NMHC, O₃, temperature, and humidity. Important NO_x reaction pathways have been preserved so that the final condensed scheme is able to handle more polluted chemical regimes as well. The condensed DMS mechanism consists of only 12 sulfur species and 33 reactions. The combination of the modified CBM4 and condensed DMS mechanisms is nearly 66% faster than the modified CBM4 and comprehensive DMS mechanism, and predicts SO₂, H₂SO₄, MSA, NO_x, and O₃ concentrations within 5-15% from the full mechanism under typical marine air conditions.

Langner *et al.* (1992) estimate that most sulfur oxidation occurs in clouds. In the simple chemistry module the aqueous phase transformation of S(IV) to SO₄⁻ is assumed to proceed through reactions with H₂O₂ and O₃. Reactions with oxygen catalyzed by metals such as manganese and iron may also be of importance in areas where the concentrations of those metals are high (Penkett *et al.*, 1979; Martin, 1984). To better predict concentrations of the important aqueous-phase oxidants H₂O₂ and O₃, we have implemented the condensed aqueous-phase mechanism proposed by Pandis and Seinfeld (1989) with a detailed mass-transfer treatment for coupling the gas- and aqueous-phase chemistries. This aqueous-phase chemistry module treats 30 species and 60 reactions and includes all the important pathways

for S(IV) transformation involving reactions of S(IV) with O_3 , H_2O_2 , O_2 (catalyzed by Mn_2^+ and Fe_3^+), OH , HO_2 , SO_5^- , HSO_5^- , SO_4^- , CH_3OOH , $CH_3C(O)OOH$, NO_2 , $HCHO$ and Cl_2^- . The detailed free radical chemistry, chlorine chemistry and the chemistry of formaldehyde and formic acid are also included to better predict concentrations of the important aqueous-phase free radicals and oxidants such as OH , HO_2 and H_2O_2 . The mass-transfer model is based on the Two-Film theory which involves calculation of the liquid-side enhancement factor for fast reacting species, and allows estimation of the overall mass-transfer limitation using contributions from both gas- and liquid-side mass-transfer resistances for a given species (Astarita, 1967; Schwartz and Freiberg, 1981; Schwartz, 1988; Shi and Seinfeld, 1991).

We have begun to extend the comprehensive gas- and aqueous-phase chemical model to include treatments for secondary organic aerosol formation from photo-oxidation products of biogenic hydrocarbons such as isoprene and terpenes. In the United States alone, biogenic hydrocarbon sources are estimated to produce 30-60 Mt of atmospheric carbon annually which includes species such as isoprene and monoterpenes. Studies (Hatakeyama *et al.*, 1989; Pandis *et al.*, 1991) have indicated significant aerosol forming potential of monoterpenes which may play an important role in CCN activation dynamics. Novakov and Penner (1994) found that organic material is a significant component of marine CCN.

Based on the available kinetic and mechanistic information for α -pinene, we have parameterized a reaction mechanism capable of producing aerosol under different atmospheric scenarios, as well as generating ozone, CO , H_2O_2 , and other gaseous products. In this scheme, α -pinene can react with OH and nitrate radical to form aerosol precursors in the presence of HO_2 radicals. Reaction of α -pinene with ozone does not contribute to aerosol formation directly, but the resulting Criegee intermediates yield the oxidants OH radical, HO_2 radical, and H_2O_2 , thus influencing the oxidant cycle and aerosol precursor oxidation rates. Typical aerosol yield from OH reaction is about 2-8% in the daytime, while that from NO_3 reaction peaks at nighttime in the range of 5-15%, depending strongly on the NO_x concentrations. Another major product in α -pinene oxidation is pinonaldehyde which can further react similarly to a typical higher aldehyde. Due to lack of data for other monoterpenes, and since α -pinene is the most dominant monoterpene emitted in the atmosphere, all monoterpenes will be modeled as α -pinene. The reaction mechanism has also been partially incorporated into the simple chemistry model. It treats formation of the secondary organic

aerosols but ignores the effects of photo-oxidation products on oxidant chemistry, and is limited to daytime conditions.

Table 1 summarizes the simple and comprehensive chemistry mechanisms.

2.5 Condensational growth and water uptake

Once oxidized, the aerosol precursor gases condense upon preexisting aerosols. Characteristic times for gas- and aerosol-phases to reach equilibrium may range from a few seconds to a few hours or even a day depending on the ambient temperature and particle size and number concentration (Wexler and Seinfeld, 1990; Meng and Seinfeld, 1996). Some field measurements appear to support the theoretically predicted time-scales (Allen and Harrison, 1989; Harrison and Msibi, 1994). Also, with several co-existing aerosol modes with different compositions, number concentrations, and mean particle diameters, the rates of condensation/evaporation to/from each will be different. This can result in preferential condensation of non-volatile gases such as sulfuric acid and MSA onto one mode over another. This effect is experienced by volatile species such as nitric and hydrochloric acids as well, along with inter-mode transfer, both governed by equilibrium constraints.

Considering these factors, we have developed a dynamic aerosol growth model suitable for global simulations. Depending on the composition, ambient RH, and particle history, the aerosol may be completely solid, completely liquid, or a mixed-phase. We plan to simulate these phases and the hysteresis effect based on individual deliquescence RHs of each salt that may form in the aerosol, at or above which it is completely dissolved while completely solid otherwise. An assumed mutual crystallization RH of 35% is used to complete the hysteresis cycle. This approach is based on several single-particle laboratory experiments (Spann and Richardson, 1985; Chan *et al.*, 1992; Tang and Munkelwitz, 1993; Tang and Munkelwitz, 1994; Kim *et al.*, 1994) as well as some field observations (Rood *et al.*, 1987; Rood *et al.*, 1989; Shaw and Rood, 1990). Thus, the equilibrium surface concentrations of each condensing/evaporating species and for each mode are estimated using equilibrium constraints depending on the ambient RH, phase-state, and the composition of the aerosol-phase. Since water vapor will always be in great excess compared to other trace gases, it is assumed to be in equilibrium with the aerosol-phase whenever a wet aerosol is predicted. We are employing the widely accepted "ZSR mixing rule" (Zdanovskii, 1936; Stokes and

Robinson, 1966, Kim *et al.*, 1993) along with the Kelvin Effect (Pruppacher and Klett, 1978) to compute the equilibrium water content of multicomponent aqueous aerosols. The Kelvin Effect is, however, ignored for the coarse mode particles.

As apparent in the above approach, the liquid-solid equilibria are ignored and thus the amounts of solid and liquid phases computed are an approximation to the actual values. However, due to the complex nature of the problem, and even more due to the fact that “real” ambient aerosols are probably much more chemically complicated, the accurate equilibrium calculation of the solids and liquids in our “simplified” system may not justify the extra computational cost.

The activity coefficients in the multicomponent aqueous aerosol are estimated by a modified version of the method proposed by Meissner and Kusik (1978). The original method was intended only for mixtures of strong electrolytes, and thus could not be used directly due to the presence of HSO_4^- , a weak acid. The binary activity coefficients of each electrolyte as a function of ionic strength are estimated by the most reliable method available for that electrolyte, including the methods of Bromley (1973), Edwards *et al.*, (1978), and Clegg and Brimblecombe (1995). The box-model version is currently being tested for speed and accuracy, and will soon be incorporated into GChM.

In the hysteresis region (humidities between the crystallization and deliquescence RHs), aerosol water content depends on the particle history. Rigorous treatment of this in the global model would require simulating both dry (solid) and wet (liquid) particles, at a major computational cost. Instead we have implemented an approximate treatment. The water content for each aerosol mode is treated as a prognostic (transported) model species. For humidities in the hysteresis region, the equilibrium water content is computed at each time step, assuming that the particles are all wet. If the transported water content exceeds 50% of this equilibrium water content, then the particles are assumed to have been wet at the previous time step, and the transported water content value is set to this equilibrium value. Otherwise the particles are assumed to have been dry and the water content is set to zero.

2.6 Activation of aerosols as CCN

We have generalized the aerosol activation parameterization of Ghan *et al.* (1993) to the case of an internal mixture of aerosol species for each mode, with different modes externally

mixed and competing as CCN (Ghan *et al.*, 1995). We have also refined the parameterization for single aerosol types by combining the strengths of the Twomey (1959) and Ghan *et al.* (1993) approaches (Abdul-Razzak *et al.*, 1997), and have generalized the refined parameterization to the multimode case. We have applied the multimode aerosol activation parameterization to the PNNL version of CCM2, with subgrid variations in activation accounted for by integrating the activation over the subgrid probability distribution of vertical velocity. The subgrid variance of vertical velocity is determined from the turbulent kinetic energy predicted in the model (Yamada and Mellor, 1979). The simulation of droplet number with prescribed aerosol concentration is broadly consistent with observations, and the simulated planetary albedo is in excellent agreement with observations.

2.7 Scattering and absorption of radiation

To estimate direct radiative forcing by aerosols, we have in the past used Kohler theory to represent the influence of relative humidity on aerosol size, and Mie theory to determine aerosol radiative properties. This physically-based approach provides the flexibility to treat a wide range of internal mixtures of aerosol components. However, the Kohler theory does not account for hysteresis in water uptake by aerosols, or interactions between ions. We have therefore introduced a much more general treatment of thermodynamic equilibrium for the gas-aerosol-water system. This treatment is described in section 2.5.

Previous efforts to estimate direct radiative forcing by aerosols have either neglected the direct radiative forcing when clouds are present (which underestimates the direct radiative forcing) or have ignored clouds altogether (which overestimates the direct radiative forcing). We have developed a method that correctly accounts for the direct radiative forcing of aerosols in the presence of clouds. By calculating the whole-sky planetary radiation balance twice each time step, once with and once without aerosols, the direct radiative forcing due to the aerosols can be determined from the difference between the whole-sky planetary radiation balance. The indirect radiative forcing requires separate simulations in which clouds are permitted to interact with the aerosols, so that the indirect radiative forcing is the difference between the total radiative forcing (the difference between the planetary radiation balance for simulations with and without anthropogenic aerosols) and the direct radiative forcing. Although calculating the whole-sky planetary radiation balance twice each time step adds an

additional computational burden to the model, we consider it worthwhile because it allows us to correctly distinguish between direct and indirect radiative forcing.

Work by Tegen *et al.* (1996) at NASA GISS has indicated that the infrared trapping by dust can be as important as the solar scattering. We have therefore applied Mie theory to estimate the infrared specific absorption by all aerosol modes, and parameterized the specific absorption in terms of the wet mode radius and wet refractive index of each mode. The influence of all aerosol modes on the upward and downward infrared flux is calculated at all model levels by assuming the aerosols act as grey body absorbers using the aerosol radiative properties at the 10 μm water vapor window (Thompson *et al.*, 1987). To determine the direct radiative forcing, the outgoing longwave flux at the top of the atmosphere is calculated twice for the same clouds, water vapor, and temperature profile: once with and once without aerosol absorption and emission.

Photolysis rates, which drive the photochemistry, are dependent on the local actinic flux, and the actinic flux generally depends upon the presence of clouds. Previously the effect of clouds on photolysis rates was ignored. The photolysis rates were computed offline as functions of altitude and solar zenith angle using clear sky values of actinic flux, and these values were curve-fit using mixed transcendental-polynomial functions.

Because cloud radiative properties are nearly independent of wavelength for visible and ultraviolet wavelengths, the influence of clouds on actinic flux (and thus photolysis rates) can be easily accounted for by using the climate model radiation code to calculate the UV actinic flux (readily determined from the direct beam and upward and downward diffuse flux) with and without clouds, and applying the ratio of the whole-sky / clear-sky actinic flux to the clear-sky photolysis rates. This is a first-order approximation because the whole-sky/clear-sky actinic flux ratio has some wavelength dependence across the UV but is only calculated at a single UV wavelength. However, this approach provides much more realistic values for the photolysis rates than was previously done, and permits an estimate of the indirect effect of aerosols on photochemistry.

2.8 Computational Performance

The computational burden of the detailed chemical mechanism is considerable. The table below lists the CPU time for the coupled model with the simple chemistry and detailed

mechanisms. The CPU time for the climate model is 0.3 and 1.8 CPU days per month at R15 and T42 resolution, respectively. The CPU time for the detailed mechanism is taxing at R15 resolution and unacceptable at T42 resolution. We have therefore parallelized the aerosol-chemistry model using a domain-decomposition method, in which the global domain is decomposed into sets of latitude bands, with one set for each processor. For optimum speed-up, the processors must have evenly distributed computational loads. Primary factors affecting the computational load include number of daytime vs. nighttime grid cells, number of cloudy vs. clear cells, and number of polluted vs. clean cells. By carefully selecting the latitude bands within each set, the computational load can be evenly distributed among processors. The latitude bands within a set need not be adjacent to each other. This has reduced the CPU-time of the model with detailed chemistry by a factor of 3.5; further reductions in CPU-time will require parallelization of the climate model.

CPU Days (IBM RS-6000-590) Per Simulated Month

R15 Resolution		T42 Resolution	
Simple Chemistry	Detailed Chemistry	Simple Chemistry	Detailed Chemistry
1.0	11.3	6.1	50.0

Additional significant speed-ups have also been achieved by implementing a regime-dependent chemistry approach (Jacobson, 1995). The gas-phase chemistry routine has been modified to allow different sets of chemistry for different chemical regimes (remote marine, continental rural, urban, mid-tropospheric, etc). The marine chemistry set is more detailed in DMS chemistry as opposed to an urban or continental rural chemistry set, which is more detailed in NMHC reactions. There are also mixed chemistry sets for handling overlapping chemical regimes. This approach reduces unnecessary complexity not demanded by a given regime, thus reducing the total computational burden. Criteria for switching between regimes have been developed. Without this treatment the timing for the detailed chemistry listed in the above table would be much worse.

3. Evaluation

For evaluating the simulated aerosols and cloud-aerosol interactions, we have applied a simple form of four-dimensional data assimilation to the coupled model so that the simulated

meteorology will follow actual meteorology during the evaluation period. The simulated winds are nudged toward ECMWF analyzed winds with a nudging time scale of about 12 hours. Temperature is also nudged to maintain thermal wind balance. The simulation described here is performed at T42 spectral resolution and with 24 vertical levels for the period June - August 1994. This period was selected on the basis of the increasing availability of multi-filter rotating shadowband radiometers (MFRSR) at a variety of sites around the world, providing accurate measurements of column aerosol optical depth under clear skies. The simple chemistry mechanism is employed. All aerosol modes (Aitken mode sulfate and carbonaceous, accumulation mode sulfate and carbonaceous, coarse dust, and sea salt) are treated.

Figure 2 compares the simulated and observed July 1994 mean surface sulfate concentration at IMPROVE and CASTNET sites in the United States, AEROCE sites in the North Atlantic, and EMEP sites in Europe. Values are averaged over all sites in selected regions, namely Scandinavia, the rest of Europe, North Atlantic, Eastern United States, Western United States, Alaska and Hawaii. The agreement is to within 20% for all regions except for the Eastern United States, where the simulated sulfate concentrations are about 40% lower than observed. The spatial correlations between simulated and observed sulfate concentrations within each region, also shown in Figure 2, are quite high for Scandinavia and the Eastern United States, but low for the rest of Europe, for the North Atlantic, and for the Western United States.

Figure 3 compares the August 1994 mean aerosol optical depth as simulated and as estimated from AVHRR radiance data (Wagener *et al.*, 1997). The simulated data have been filtered by a mask consistent with the AVHRR analysis, which cannot estimate aerosol optical depth at night, under cloudy conditions, or over land. Note that during August 1994 the NOAA satellite orbit carried the AVHRR instrument over the southern hemisphere in darkness, so that no estimates of aerosol optical depth are possible there. The model is correctly simulating the low aerosol optical depths over the remote oceans and the aerosol plumes flowing eastward from the northeastern United States and westward from the Saharan Desert. The high optical depths in the Middle East are also simulated well. However, the model overestimates the optical depth in the central north Atlantic Ocean and off the coast of Norway.

Figure 4 compares the July – August mean aerosol optical depth as simulated and as measured at 18 surface MFRSR and stellar observatory sites. Because aerosol optical depth cannot be measured under cloudy conditions, both simulated and observed optical depths are averaged only for clear-sky conditions. The surface measurements and the simulated optical depth agree to within 0.05 for nearly all sites, and little bias is apparent. The one outlier is the stellar observatory at Uzbekistan, where the simulated optical depth is much higher than observed, probably because the observatory is located on a mountaintop, above most of the pollution present over an area the size of a model grid cell. The same explanation also applies to Mauna Loa. A more appropriate comparison between simulated and observed optical depths would account for the difference between the model grid cell surface elevation and the elevation of the surface site, and this will be done in future evaluations.

How well does the global model represent cloud-aerosol interactions? Figure 5 compares the simulated and observed relationship between droplet number and aerosol number. The ratio of the droplet number to aerosol number is plotted versus the aerosol number. The observations are from aircraft measurements reported by Gillani *et al.* (1992). The simulated values, which are derived from monthly means at all grid points, have been adjusted to account for the minimum particle size measured by the instrument. Both the simulation and the observations show that the ratio decreases with increasing aerosol concentration, reflecting the greater competition among cloud condensation nuclei at higher aerosol concentrations. The simulated ratio is generally smaller than that observed for the same aerosol concentration, indicating that the model underestimates droplet number given an aerosol concentration. Cloud simulations with a single column model suggest that this underestimation is probably due to inadequate vertical resolution in the global model (Ghan *et al.*, 1997).

Figure 6 compares the simulated and observed frequency distributions of droplet number for marine and continental air. The model correctly predicts the smaller droplet number concentrations and narrower frequency distribution for marine air, but generally underestimates continental droplet concentrations.

In spite of simulating droplet number concentrations which are somewhat too low, the model does simulate the planetary radiation balance quite well. Figure 7 compares the

simulated and observed July mean cloud radiative forcing. The simulation captures the primary spatial variations in cloud radiative forcing. The shortwave cloud radiative forcing is too strong in the Intertropical Convergence Zone, but this error is more an artifact of the nudging scheme than of errors in model physics because it vanishes when nudging is not applied. The global mean shortwave cloud forcing is too strong by about 10 W m^{-2} , even though simulated droplet number concentrations are probably too low.

4. Application to Climate Forcing

Having performed a preliminary evaluation of the the global aerosol model, we now apply it to the problem of estimating the direct and indirect radiative forcing due to anthropogenic sulfate. The total radiative forcing is determined from the difference in the planetary radiation balance for two simulations, one with and one without anthropogenic sulfate. Direct forcing is estimated by calculating the solar radiation balance twice during the same simulation, once with aerosols and once without, with the direct forcing due to anthropogenic sulfate determined from the difference between the direct forcing for the two simulations. That is, if S and S_{clean} are the solar flux calculated with and without aerosols, respectively, for a particular simulation, then the direct forcing given by $D = \Delta(S - S_{clean})$. Direct longwave forcing is neglected because it is thought to be relatively small for sulfate aerosols. Indirect forcing due to anthropogenic sulfate is determined from the difference between the total radiative forcing for the two simulations, and the direct forcing due to anthropogenic sulfate: $I = \Delta S - D = \Delta S_{clean}$.

Because they are preliminary, the simulations are performed at the relatively coarse R15 resolution. The simulated winds and temperature are, like the evaluation simulation, nudged toward ECMWF analyses. Without such nudging, the simulated winds are not accurate enough for the treatment of dust emission, which is highly sensitive to surface wind speed. In addition, nudging reduces the influence of dynamical instabilities on natural variability, so that differences between simulated fields can be more accurately attributed to differences in model physics.

Table 2 compares the simulated and observed global mean planetary radiation balance for July 1994. The simulated global radiation balance is within 10 W m^{-2} for the longwave. The simulated shortwave cloud forcing is about 15 W m^{-2} too strong, primarily due to an

excessively strong simulated intertropical convergence zone. At other latitudes the agreement with observations is quite good.

The simulated direct forcing due to anthropogenic sulfate is estimated to be -0.7 W m^{-2} , which is in agreement with other estimates, allowing for the fact that the simulation was performed for the summertime of the more polluted northern hemisphere. The indirect forcing due to anthropogenic sulfate is -2.4 W m^{-2} , substantially stronger than other more empirically-based estimates. The annual mean indirect forcing is likely to be somewhat weaker. Treating more organic aerosols could further reduce the indirect forcing estimate by increasing the competition among CCN, but the estimated indirect forcing is unlikely to be reduced by more than a factor of two.

Figure 8 shows the the zonal mean direct forcing for the simulations with and without anthropogenic sulfur. The direct forcing is positive over the arctic, where the surface albedo is higher than the albedo of the smoke. The anthropogenic sulfur contributes to direct forcing most in the northern midlatitudes, with fairly uniform cooling of about 20 W m^{-2} between 30N and 70N.

The indirect forcing is partly due to the smaller size of the cloud droplets with anthropogenic sulfur, and partly due to the greater liquid water. Figure 9 shows the spatial frequency distributions of in-cloud droplet number concentration for the two simulations. The distributions look similar, but there is a systematic difference between the distributions, the median droplet number concentration being 47.8 and 40.5 cm^{-3} for the simulations with and without anthropogenic sulfur. Such a shift produces differences in both droplet effective radius and column liquid water. The median effective radius decreases from 11.1 μm without anthropogenic sulfur to 10.7 μm with anthropogenic sulfur. The global mean column liquid water increases from 70.5 g m^{-2} without anthropogenic sulfur to 73.5 g m^{-2} with anthropogenic sulfur, with most of the increase occurring in the more polluted hemisphere. The cloud fraction, suggested by some to increase with more pollution, changes very little.

5. Future Work

We have developed the global aerosol model to the point that several publications are in sight. These include

- A paper comparing the simulated and observed surface sulfate and aerosol optical depth. The simulation has already been performed and much of the analysis is complete.
- A paper exploring the sensitivity of the simulated direct and indirect radiative forcing to an assumed background aerosol concentration. Simulations with background aerosol concentrations of 100 and 300 cm^{-3} are under way.
- A paper estimating the direct and indirect radiative forcing. The preliminary R15 June-July simulations will be extended to T42 resolution and a full annual cycle.
- A paper comparing simulations with detailed and simple chemistry. Both models are nearly ready to begin two-month simulations at R15 resolution.
- A paper evaluating the CO simulation by comparing with MAPS measurements during April and October 1994.

If the last paper shows that the detailed chemistry makes little difference in the simulated aerosol optical depth and CCN concentrations, then our future work will focus on the prediction of aerosol number in the simple chemistry model. If, on the other hand, the comparison shows that the detailed chemistry yields substantially different aerosol optical depth and CCN concentrations, then our future work will include a significant effort on improving the computational efficiency of the detailed chemistry model and performing more simulations with it. All this work of course, will be funded by our new NASA MTPE Grant and by support from the DOE Atmospheric Chemistry program.

6. Publications

- Saylor, R.D., and G.D. Ford, 1995: On the comparison of numerical methods for the integration of kinetic equations in atmospheric chemistry and transport models. *Atmos. Environ.*, 29, 2585-2593.
- Abdul-Razzak, H., S.J. Ghan, and C. Rivera-Carpio, 1997: A parameterization of aerosol activation. Part I: Single aerosol type. *Atmos. Res.*, accepted.

- Saylor, R. D., R. C. Easter, E. G. Chapman, 1997: Simulation of the tropospheric distribution of carbon monoxide during the 1984 MAPS experiment. *J. Geophys. Res.*, submitted.
- Ghan, S.J., L.R. Leung, R.C. Easter, and H. Abdul-Razzak, 1997: Prediction of droplet number in a general circulation model. *J. Geophys. Res.*, submitted.
- Ghan, S.J., R.C. Easter, Y. Zhang, L.R. Leung, R.D. Saylor, L.K. Peters, R. Zaveri, and P. Lee, 1997: Radiative forcing of climate by aerosols: A physically based modeling approach. *Proceedings of the Third AMS Conference on Atmospheric Chemistry*, Long Beach CA, February 1997.
- Ghan, S.J., R.C. Easter, L.R. Leung, and Y. Zhang, 1995: Global simulation of cloud-aerosol interactions. *EOS, 76, Transactions of the 1995 Fall AGU Meeting*. American Geophysical Union.
- Ghan, S.J., R.C. Easter, L.R. Leung, R.D. Saylor, C.M. Berkowitz, and L.K. Peters, 1995: Global simulation of cloud-aerosol interactions. *IUGG XXI General Assembly*, Boulder CO, July 1995.

References

- Abdul-Razzak, H., S.J. Ghan, and C. Rivera-Carpio, 1997: A parameterization of the fraction of activation of atmospheric aerosols. *Atmos. Res.*, accepted.
- Allen, A. G. and R. M. Harrison 1989: Field measurements of the dissociation of ammonium nitrate and ammonium chloride aerosols. *Atmos. Environ.*, *23*, 1591-1599.
- Astarita G., 1967: *Mass transfer with chemical reaction*. Elsevier, New York.
- Benkovitz, CM, M. Trevor Scholtz, J. Pacyna, L. Tarrason, J. Dignon, E.C. Voldner, P.A. Spiro, J.A. Logan and T.E. Graedel, 1996: Global gridded inventories of anthropogenic emissions of sulfur and nitrogen, *J. Geophys. Res.*, *101*, (29,239-29,253).
- Bromley, L. A., 1973: Thermodynamic properties of strong electrolytes in aqueous solutions. *AIChE J.*, *19*, 313-320.
- Chan, C. K., R. C. Flagan, and J. H. Seinfeld, 1992: Water activities of $\text{NH}_4\text{NO}_3/(\text{NH}_4)_2\text{SO}_4$ solutions. *Atmos. Environ.*, *26A*, 1661-1673.
- Clegg, S. L. and P. Brimblecombe 1995: A generalised multicomponent thermodynamic model applied to the $(\text{NH}_4)_2\text{SO}_4 - \text{H}_2\text{SO}_4 - \text{H}_2\text{O}$ system to high supersaturation and low relative humidity at 298.15 K. *J. Aerosol Sci.*, *26*, 19-38.
- Corchnoy S.B. and R. Atkinson, Kinetics of the gas-phase reactions of OH and NO₃ radicals with 2-carene, 1,8-cineole, p-cymene, and tepinylene, *Environ. Sci. Technol.*, *24*: 1497-1502, 1990.
- Covert, D. S., 1995: Aerosol number size distributions from 3 to 500 nm diameter in the summer Arctic marine boundary layer. *Tellus B*, accepted.
- Dentener, F.J. and P.J. Crutzen, A three-dimensional model of the global ammonia cycle, *J. Atmos. Chem.*, *19*, 331-369, 1994.
- Eagan, R. C., P. V. Hobbs, and L. F. Radke, 1974: Measurements of cloud condensation nuclei and cloud droplet size distributions in the vicinity of forest fires. *J. Appl. Met.*, *13*, 553-559.
- Easter, R. C., R. D. Saylor, and E. G. Chapman (1994) Analysis of mid-tropospheric carbon monoxide data using a three-dimensional global atmospheric chemistry numerical model, in *Air Pollution Modeling and Its Application X*, ed. S.V. Gryning and M. M. Millan, Plenum Press, New York.

- Edwards, T. J., G. Maurer, J. Newman, and J. M. Prausnitz 1978: Vapor-liquid equilibria in multicomponent aqueous solutions of volatile weak electrolytes. *AIChE J.*, *24*, 966-976.
- Erickson, D. J., and R. A. Duce. 1988. On the global flux of atmospheric sea-salt. *J. Geophys. Res.* *93*, 14079-14088.
- Friedlander, S. K., 1977: *Smoke, Dust and Haze*. John Wiley and Sons, New York.
- Gelbard, F. and J. H. Seinfeld, 1980: Simulation of multicomponent aerosol dynamics. *J. Colloid Interface Sci.*, *78*, 485-501.
- Gery M. W., Whitten G. Z., Killus J. P. and Dodge M. C., 1989: A photochemical kinetics mechanism for urban and regional scale computer modeling. *J. Geophys. Res.* *94*, 12,925-12,956.
- Ghan, S.J., and L.R. Leung, 1996: Prediction of droplet number in a general circulation model. *J. Geophys. Res.*, submitted.
- Ghan, S.J., C.C. Chuang, R.C. Easter, and J.E. Penner, 1995: A parameterization of cloud droplet nucleation. Part II: Multiple aerosol types. *Atmospheric Research*, *36*, 39-54.
- Ghan, S.J., C.C. Chuang, and J.E. Penner, 1993: A parameterization of cloud droplet nucleation. Part I: Single aerosol type. *Atmospheric Research*, *30*, 197-222.
- Ghan, S.J., L.R. Leung, R.C. Easter, and H. Abdul-Razzak, 1997: Prediction of cloud droplet number in a general circulation model. *J. Geophys. Res.*, submitted.
- Gillani, N.V., P.H. Daum, S.E. Schwartz, W.R. Leitch, J.W. Strapp, and G.A. Isaac, 1992: Fractional activation of accumulation-mode particles in warm continental stratiform clouds. In *Precipitation Scavenging and Atmosphere-Surface Exchange*, S.E. Schwartz and W.G.N. Slinn (Eds.), Hemisphere Publ., Washington, D.C., pp. 345-358.
- Gillette D.A. and Passi R., 1988: Modeling dust emission caused by wind erosion. *J. of Geophysical Research*, *93*, 14,233-14,242.
- Giorgi, F., 1986: *Development of an atmospheric model for studies of global budgets and effects of airborne particulate material*. Ph. D. Thesis, Cooperative Thesis No. 102, Georgia Institute of Technology, Atlanta, GA, and National Center for Atmospheric Research, Boulder, Colorado.
- Graedel, T. E., 1994: Global emissions inventories to aid atmospheric modelers, *Eos Trans. AGU*, *75*, 585-591.
- Guenther, A., C.N. Hewitt, D. Erickson, R. Fall, C. Geron, T. Graedel, P. Harley, L. Klinger,

- M. Lerdau, W.A. McKay, T. Pierce, B. Scholes, R. Steinbrecher, R. Tallamraju, J. Taylor, and P. Zimmerman, 1995: A global model of natural volatile organic compound emissions. *J. Geophys. Res.*, *100*, 8873–8892.
- Hallberg, A., J.A. Ogren, K.J. Noone, K. Okada, J. Heintzenberg, and I.B. Svenningsson, 1994: The influence of aerosol particle composition on cloud droplet formation. *J. Atmos. Chem.*, *19*, 153-171.
- Hao, W. M., M.-H. Liu, and P. J. Crutzen (1990) Estimates of annual and regional releases of CO₂ and other trace gases to the atmosphere from fires in the tropics, based on the FAO statistics for the period 1975-1980, in *Fire in the Tropical Biota: Ecosystem Processes and Global Challenges*, ed. J. G. Goldammer, pp. 440-462, Springer-Verlag, Berlin.
- Harrison, E.F., P. Minnis, B.R. Barkstrom, V. Ramanathan, R.D. Cess, and G.G. Gibson, Seasonal variation of cloud radiative forcing derived from the Earth Radiation Budget Experiment. *J. Geophys. Res.*, *95*, 18,687–18,703, 1990.
- Harrison, R. M. and I. M. Msibi 1994: Validation of techniques for fast response measurement of HNO₃ and NH₃ and determination of the [NH₃][HNO₃] concentration product. *Atmos. Environ.*, *28*, 247-255.
- Hatakeyama S., K. Izumi, T. Fukuyama, and H. Akimoto, Reactions of ozone with α -pinene and β -pinene in air: yields of gaseous and particulate products, *J. Geophys. Res.* *94*: 13013-13024, 1989.
- Hindmarsh, A. C., 1983: ODEPACK: a systematized collection of ode solvers. In *Scientific Computing* (R. S. Stepleman, ed.), pp. 55-64. North Holland Press, Amsterdam.
- Jacobson, M. Z., 1995: Computation of global photochemistry with SMVGEAR II. *Atmos. Environ.*, *29*, 2541-2546.
- Jacobson, M. Z., and R. P. Turco, 1994: SMVGEAR: A sparse-matrix, vectorized Gear code for atmospheric models, *Atmos. Environ.*, *28*, 273-284.
- Jaenicke, R., 1993: Tropospheric Aerosols. In *Aerosol-Cloud-Climate Interactions*, P.V. Hobbs (Ed.), Academic Press, 237 pp.
- Jeuken, A.B.M., P.C. Siegmund, L.C. Heijboer, J. Feitchet, and L. Bengtsson, 1996: On the potential of assimilating meteorological analyses in a global climate model for the purpose of model validation. *J. Geophys. Res.*, *101*, 16,939–16,950.
- Kalnay, E., M. Kanamitsu, R. Kistler, W. Collins, D. Deaven, L. Gandin, M. Iredell, S.

- Saha, G. White, J. Wollen, Y. Zhu, M. Chelliah, W. Ebisusaki, W. Higgins, J. Janowiak, K.C. Mo, C. Ropelewski, J. Wang, A. Leetmaa, R. Reynolds, R. Jenne, and D. Joseph, 1996: The NCEP/NCAR 40-year reanalysis project. *Bull. Amer. Meteorol. Soc.*, *77*, 437-471.
- Kim Y. P., J. H. Seinfeld, and P. Saxena, 1993: Atmospheric gas-aerosol equilibrium I. Thermodynamic model. *Aerosol Sci. Technol.*, *19*, 157-181.
- Kim Y. P., B. K.-L., Pun, C. K. Chan, R. C. Flagan, and J. H. Seinfeld, 1994: Determination of water activity in ammonium sulfate and sulfuric acid mixtures using levitated single particles. *Aerosol Sci. Technol.*, *20*, 275-284.
- Kreidenweis, S. M., and J. H. Seinfeld, 1988: Nucleation of sulfuric acid-water and methanesulfonic acid-water solution particles: Implications for the atmospheric chemistry of organosulfur species. *Atmos. Environ.*, *22*, 283-296.
- Langner, J., H. Rodhe, P.J. Crutzen, and P. Zimmermann, 1992: Anthropogenic influence on the distribution of tropospheric sulphate aerosol. *Nature*, *359*, 712-716.
- Lelieveld, J. and P. J. Crutzen, 1990: Influences of cloud photochemical processes on tropospheric ozone. *Nature* *343(18)*, 227-233.
- Liousse, C., J. E. Penner, C. R. Molenkamp, J. J. Walton, H. Edelman, I. Shult, and H. Cachier, 1994: Modeling aerosols from biomass burning. *Fifth International Conference on Carbonaceous Particles in the Atmosphere*, August 23-26, Berkeley, California.
- Malm, W. C., J. F. Sisler, D. Huffman, R. A. Eldred, and T. A. Cahill, 1994: Spatial and seasonal trends in particle concentration and optical extinction in the United States. *J. Geophys. Res.*, *99D*, 1347-1370.
- Martin, A., 1984: Estimated washout coefficients for sulfur dioxide, nitric oxide, nitrogen dioxide and ozone. *Atmos. Environ.* *18*, 1955-1961.
- Meissner, H. P., and C. L. Kusik, 1978: Electrolyte activity coefficients in inorganic processing. *AIChE Symp. Ser.*, *173*, 14-20.
- Meng, Z. and J. H. Seinfeld, 1996: Time scales to achieve atmospheric gas-aerosol equilibrium for volatile species. *Atmos. Environ.*, *30*, 2889-2900.
- Novakov, T., and J.E. Penner, 1993: Large contribution of organic aerosol to cloud condensation nuclei concentrations: Evidence from a marine site. *Nature*, *365*, 823-826.
- Pandis S.N. and Seinfeld J.H., 1989: Sensitivity analysis of a chemical mechanism for

- aqueous-phase atmospheric chemistry. *J. Geophys. Res.*, *94*, 1105-1126.
- Pandis S.N., S.E. Paulson, J.H. Seinfeld, and R.C. Flagan, 1991: Aerosol formation in the photooxidation of isoprene and beta-pinene.
- Pandis S.N., R.A. Harley, G.R. Cass, and J.H. Seinfeld, 1992: Secondary organic aerosol formation and transport. *Atmos. Environ.*, *26A*, 2269-2282.
- Penkett, S. A., Jones, B.M. R., Brice, K. A., and Eggleton, A. E. J., 1979: The importance of atmospheric ozone and hydrogen peroxide in oxidizing sulfur dioxide in cloud and rain water. *Atmos. Environ.* *13*, 123-137.
- Penner, J.E., 1995: Carbonaceous aerosols influencing atmospheric radiation: black and organic carbon. *Aerosol Forcing of Climate*. R.J. Charlson and J. Heintzenberg (Eds.), John Wiley & Sons.
- Penner, J.E., R.E. Dickinson, and C.A. O'Neill, 1992: Effects of aerosol from biomass burning on the global radiation budget. *Science*, *256*, 1432-1433.
- Penner, J.E., H. Eddleman, and T. Novakov, 1993: Towards the development of a global inventory for black carbon emissions. *Atmos. Environ.*, *27A*, 1277-1295.
- Piccot, S.D., J.J. Watson, and J.W. Jones, 1992: A global inventory of volatile organic compound emissions from anthropogenic sources. *J. Geophys. Res.*, *97*, 9897-9912.
- Pruppacher, H. R., and J. D. Klett, 1978: Microphysics of clouds and precipitation. Reidel, 141 pp.
- Rood, M. J., D. S. Covert, and T. V. Larson, 1987: Hygroscopic properties of atmospheric aerosol in Riverside, California. *Tellus*, *39B*, 383-397.
- Rood, M. J., M. A. Shaw, T. V. Larson, and D. S. Covert, 1989: Ubiquitous nature of ambient metastable aerosol. *Nature*, *337*, 537-539.
- Saylor, R. D., R. C. Easter, E. G. Chapman, 1997: Simulation of the tropospheric distribution of carbon monoxide during the 1984 MAPS experiment. *J. Geophys. Res.*, submitted.
- Schwartz S.E., 1988: Mass-transport limitation to the rate of in-cloud oxidation of SO₂: re-examination in the light of new data. *Atmos. Environ.*, *22*, 2491-2499.
- Schwartz S.E. and Freiberg J.E., 1981: Mass-transport limitation to the rate of reaction of gases in liquid droplets: application to oxidation of SO₂ in aqueous solutions. *Atmos. Environ.*, *15*, 1129-1144.

- Shaw M. A., and M. J. Rood, 1990: Measurement of the crystallization humidities of ambient aerosol particles. *Atmos. Environ.*, *24A*, 1837-1841.
- Shi B. and Seinfeld J.H., 1991: On mass-transport limitation to the rate of reaction of gases in liquid droplets. *Atmos. Environ.*, *22*, 2491-2499.
- Shorees B., R. Atkinson and Arey J., 1991: Kinetics of the gas-phase reactions of b-phellandrene with OH and NO₃ radicals and O₃ at 297·2K, Int. *J. Chem. Kinet.*, *23*: 897-906.
- Spann, J. F., and C. B. Richardson, 1985: Measurement of the water cycle in mixed ammonium acid sulfate particles. *Atmos. Environ.*, *19*, 819-825.
- Spiro, P.A., D.J. Jacobs, and J.A. Logan, 1992: Global inventory of sulfur emissions with 1°x 1°resolution. *J. Geophys. Res.*, *97*, 6023-6036.
- Stockwell W. R., 1986: A homogeneous gas-phase mechanism for use in a regional acid deposition model. *Atmospheric Environment* *20*, 1615-1632.
- Stockwell W. R., Middleton P. and Chang J.S., 1990: The second generation regional acid deposition model chemical mechanism for regional air quality modeling. *J. Geophys. Res.* *95*, 16,343-16,367.
- Stokes, R. H., and R. A. Robinson, 1966: Interactions in aqueous nonelectrolyte solutions. *J. Phys. Chem.*, *70*, 2126-2131.
- Tang, I. N., and H. R. Munkelwitz, 1993: Composition and temperature dependence of the deliquescence properties of hygroscopic aerosols. *Atmos. Environ.*, *27A*, 467-473.
- Tang, I. N., and H. R. Munkelwitz, 1994: Water activities, densities, and refractive indices of aqueous sulfates and sodium nitrate droplets of atmospheric importance. *J. Geophys. Res.*, *99*, 18,801-18,808.
- Tegen, I., A. Lacis and I. Fung, 1996: The influence on climate forcing of mineral aerosols from disturbed soils. *Nature*, *380*, 419-422.
- Thompson, S.L., V. Ramaswamy, and C. Covey, 1987: Atmospheric effects of nuclear war aerosols in general circulation model simulations: Influence of smoke optical properties. *J. Geophys. Res.*, *92*, 10,942-10,960.
- Twomey, S., 1959. The nuclei of natural cloud formation. Part II: The supersaturation in natural clouds and the variation of cloud droplet concentration. *Geophys. Pura e Applicata*, *43*:243-249.

- Wagener, R., S. Nemesure, and S. E. Schwartz, 1997: Aerosol optical depth over oceans: High space and time resolution retrieval and error budget from satellite radiometry. *J. Atmos. Oceanic Tech.* in press.
- Wallace, J.M., and P.V. Hobbs, 1977: *Atmospheric Science: An Introductory Survey*. Academic Press, New York, p. 168.
- Wexler, A. S. and J. H. Seinfeld, 1990: The distribution of ammonium salts among a size and composition dispersed aerosol. *Atmos. Environ.*, *24A*, 1231-1246 .
- Wexler, A. S. and J. H. Seinfeld, 1991: Second-generation inorganic aerosol model. *Atmos. Environ.*, *25A*, 2731-2748.
- Whitby, E. R., P. H. McMurry, U. Shankar, and F. S. Binkowski, 1991: *Modal Aerosol Dynamics Modeling*. Report to U. S. EPA, Research Triangle Park, North Carolina.
- Whitby, K. T., 1978: The physical characteristics of sulfur aerosols. *Atmos. Environ.*, *12*, 135-159.
- Yamada, T. and G.L. Mellor, 1979: A numerical simulation of BOMEX data using a turbulence closure model coupled with ensemble cloud relations. *Quart. J. Roy. Meteor. Soc.*, *105*, 915-944.
- Yin F., Grosjean D. and Seinfeld J. H., 1990a: Photooxidation of dimethyl sulfide and dimethyl disulfide. I: Mechanism development. *J. Atmos. Chem.* *11*, 309-364.
- Yin F., Grosjean D., Flagan R. C. and Seinfeld J. H., 1990b: Photooxidation of dimethyl sulfide and dimethyl disulfide. II: Mechanism evaluation. *J. Atmos. Chem.* *11*, 365-399.
- Zdanovskii, A. B., 1936: Trudy Solyanoi Laboratorii Akad. Nauk SSSR, No. 6.

Table 1. CHEMISTRY MECHANISMS

Species	Simple Mechanism	Detailed Mechanism
Sulfur	$SO_2 + OH \rightarrow H_2SO_4$	$SO_2 + OH \rightarrow H_2SO_4$
	$DMS + OH \rightarrow a.SO_2 + (1 - a).MSA$ (crude parameterization)	$DMS + OX \rightarrow SO_2 + H_2SO_4 + MSA + DMSO + DMSO_2$ (condensed mechanism with 12 species, 33 reactions)
	$S(IV) + (H_2O_2, O_3) \rightarrow SO_4^-$	$S(IV) + (H_2O_2, O_3, \text{metals}, OH, HO_2, SO_5^-, HSO_5^-, SO_4^-, CH_3OOH, CH_3C(O)OOH, NO_2, HCHO, Cl_2^-) \rightarrow SO_4^-$
Nitrate	not treated	$NO_x + OX \rightarrow HNO_3$ $N_2O_5(g) \rightarrow \text{nitrate}$ Dynamic aerosol growth model for $HNO_3 \leftrightarrow \text{nitrate}$ and $NH_3 \leftrightarrow \text{ammonium}$ NH_3 and ammonium simulated
Ammonium	Sulfate assumed to be $(NH_4)_2SO_4$	Biogenic HC + OX \rightarrow Organic Aerosol + Reactive Products (involved in gas phase oxidant chemistry)
Organics	Biogenic HC + OH \rightarrow Organic Aerosol	$NMHC + OX \rightarrow \text{Organic Aerosol} + \text{Reactive Products}$
Oxidants	OH and H_2O_2 predicted O_3 and NO_x prescribed Gas phase CO - CH_4 chemistry	All oxidants and NO_x predicted Gas phase CO, CH_4 , $NMHC$, and Biogenic HC chemistry (CBM4 with CH_4 , C_2H_6 , isoprene, monoterpenes, and associated radicals added)
	Aqueous loss of H_2O_2 (reaction with S(IV))	Aqueous free radical, chlorine, and HCHO chemistry (30 species and 60 reactions)

** OX = oxidant species (OH, HO_2 , O_3 , NO_3 , ...)

Table 2. GLOBAL RADIATION BALANCE

	Observed	Simulated		Δ
	July	anthro	natural	
Outgoing Longwave				
cloud-free sky	264.6	271.3	271.3	0.0
cloud forcing	28.4	28.6	28.7	-0.1
total	239.1	242.6	242.7	-0.1
Absorbed Solar				
cloud-free sky	280.8	284.8	286.0	-1.2
cloud forcing	-46.3	-62.1	-60.3	-1.8
total	234.5	222.7	225.8	-3.1
clean sky		223.9	226.3	-2.4
total - clean		-1.2	-0.5	-0.7
Net ERB				
cloud-free sky	16.2	13.5	14.7	-1.2
cloud forcing	-20.8	-33.4	-31.6	-1.8
total	-4.6	-19.9	-16.9	-3.0

Figures

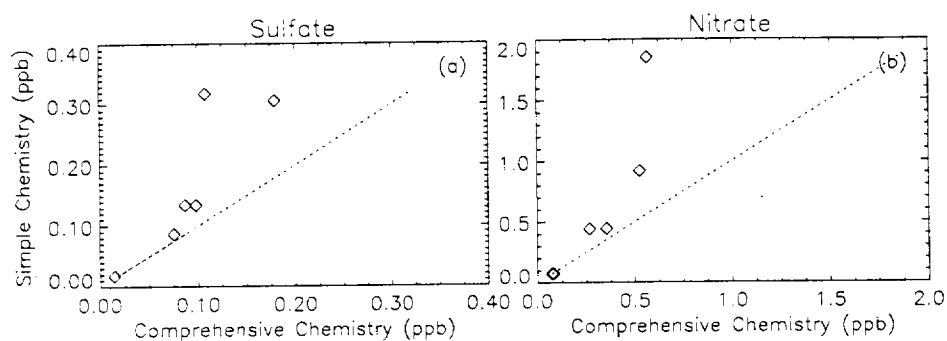


Figure 1: Box-model comparison between performances of simple and comprehensive chemical mechanism for sulfate and nitrate productions. Note that simple chemistry tends to predict higher sulfate and nitrate concentrations under a range of rural conditions. The sulfate and nitrate are actually H_2SO_4 and HNO_3 , which would condense onto aerosols. The simple mechanism simulates HNO_3 very crudely (in steady state with the prescribed NO_x concentrations), and we do not actually use this HNO_3 to produce nitrate aerosol in the global aerosol-chemistry model.

Figure 2: Simulated and observed July 1994 mean surface sulfate concentration in selected regions.

Figure 3: August 1994 mean aerosol optical depth as simulated and as estimated from AVHRR radiance data.

Figure 4: July–August 1994 mean aerosol optical depth as simulated and as measured by multifilter rotating shadowband radiometers and stellar photometry.

Figure 5: Simulated and observed ratio of the droplet number to aerosol number plotted versus the aerosol number concentration. Observations are from aircraft measurements by Gillani *et al.* (1992). Simulated values are time means at each grid point, with aerosol number concentrations reduced to account for the minimum particle size measured by the aircraft instrument.

Figure 6: Simulated and observed frequency distributions of droplet number for marine and continental air. Observations are from *Tellus 10*, 258–259 as reported by Wallace and Hobbs (1977). Simulated values are for time means at each grid point.

Figure 7: Zonal mean longwave and shortwave cloud forcing simulated and observed for July. Observations are from Harrison *et al.* (1990).

Figure 8: Zonal mean direct radiative forcing by all aerosols and by all but the anthropogenic sulfate aerosols for July.

Figure 9: Spatial frequency distributions of the July mean in-cloud droplet number concentration for simulations with and without anthropogenic sulfur.

Observed and Simulated Surface Sulfate Concentrations for July 1994

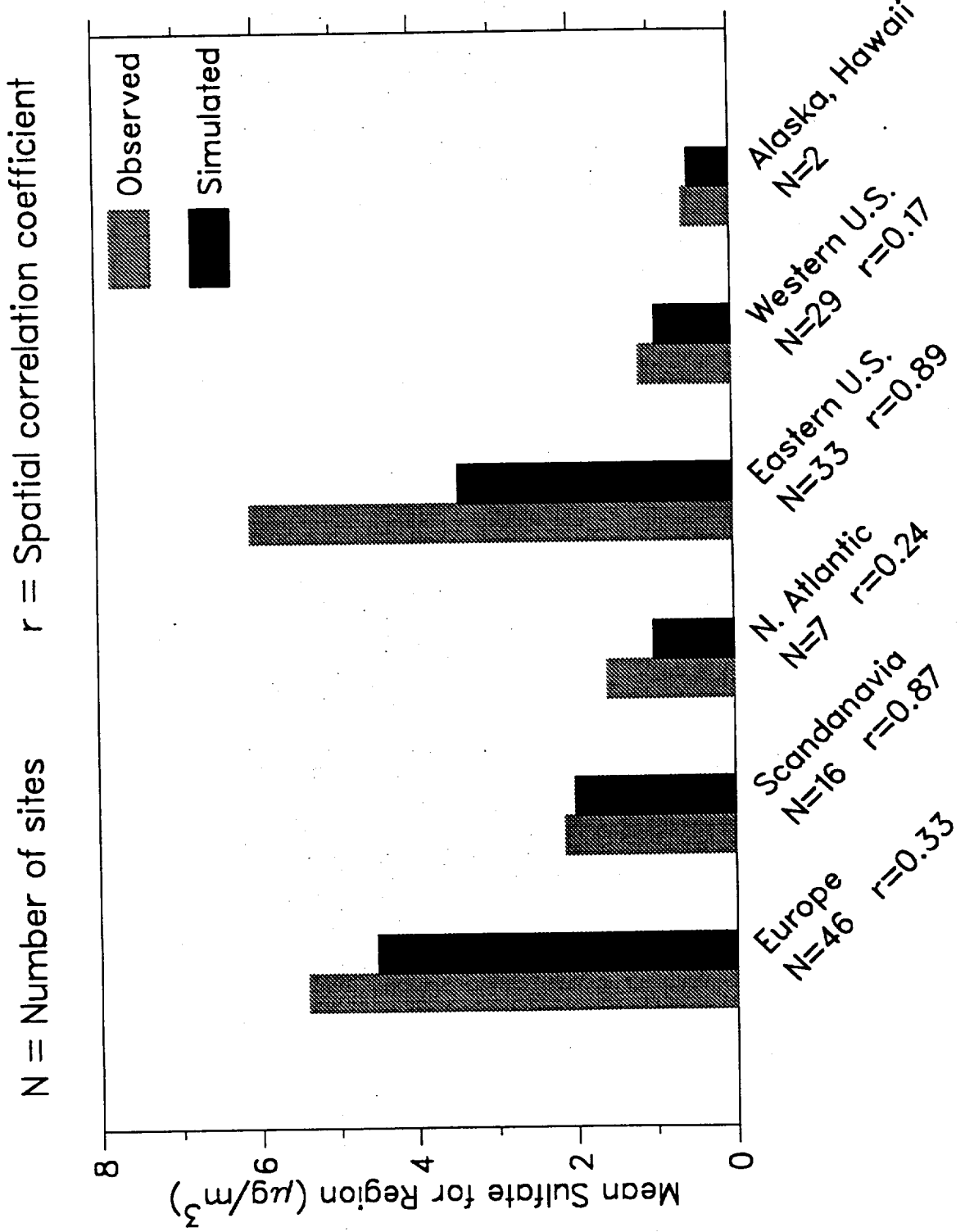
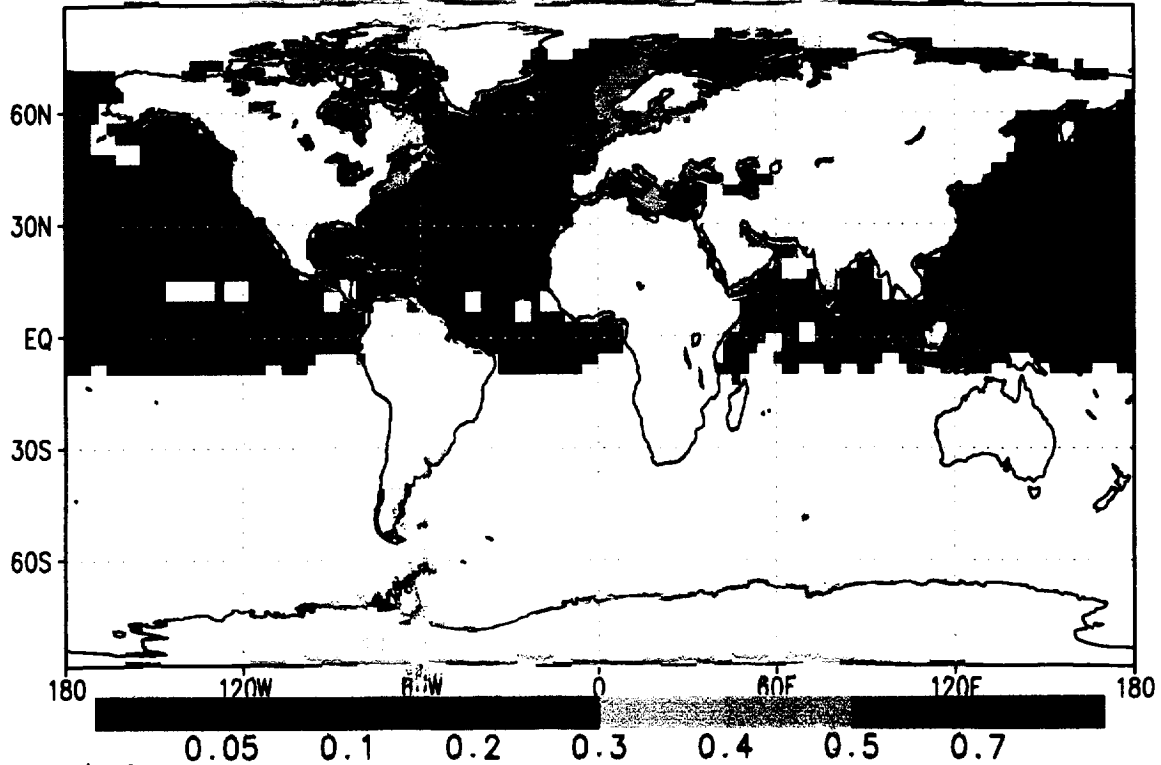


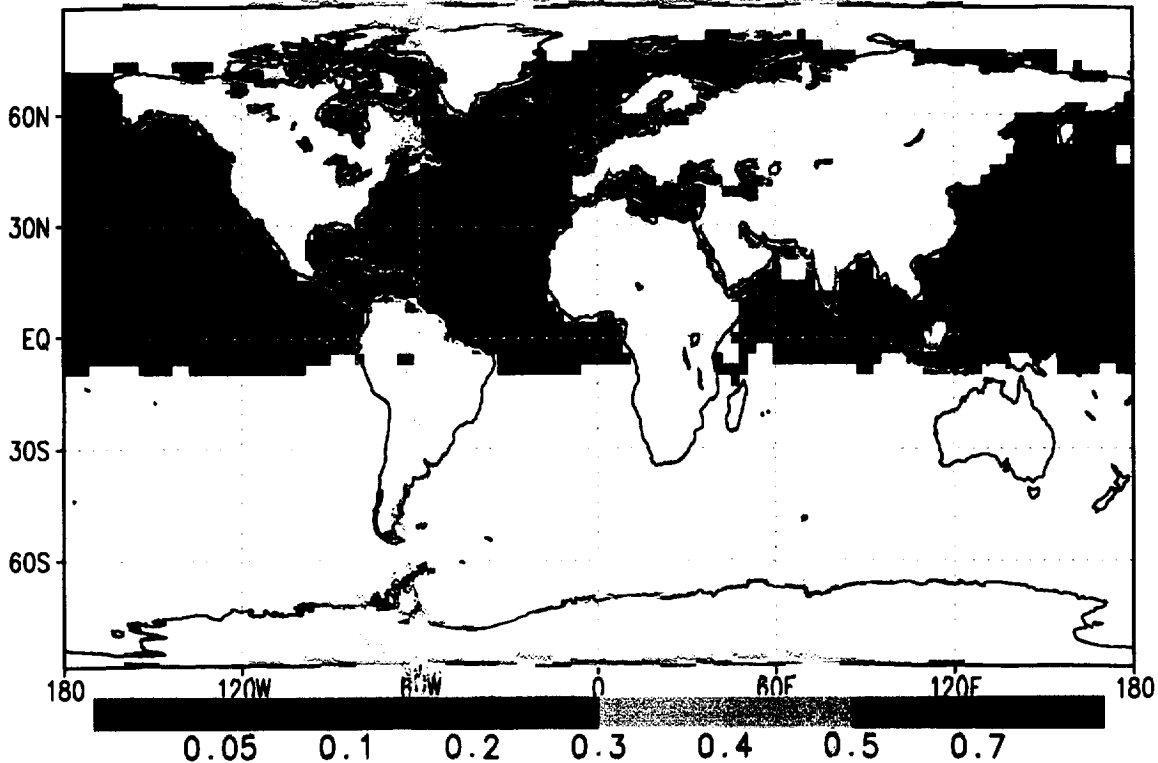
Fig. 2

SIMULATED AEROSOL OPTICAL DEPTH



GrADS: COLA/UMCP

OBSERVED AEROSOL OPTICAL DEPTH



GrADS: COLA/UMCP

Simulated vs. Observed Aerosol Optical Depth
for Surface Sites

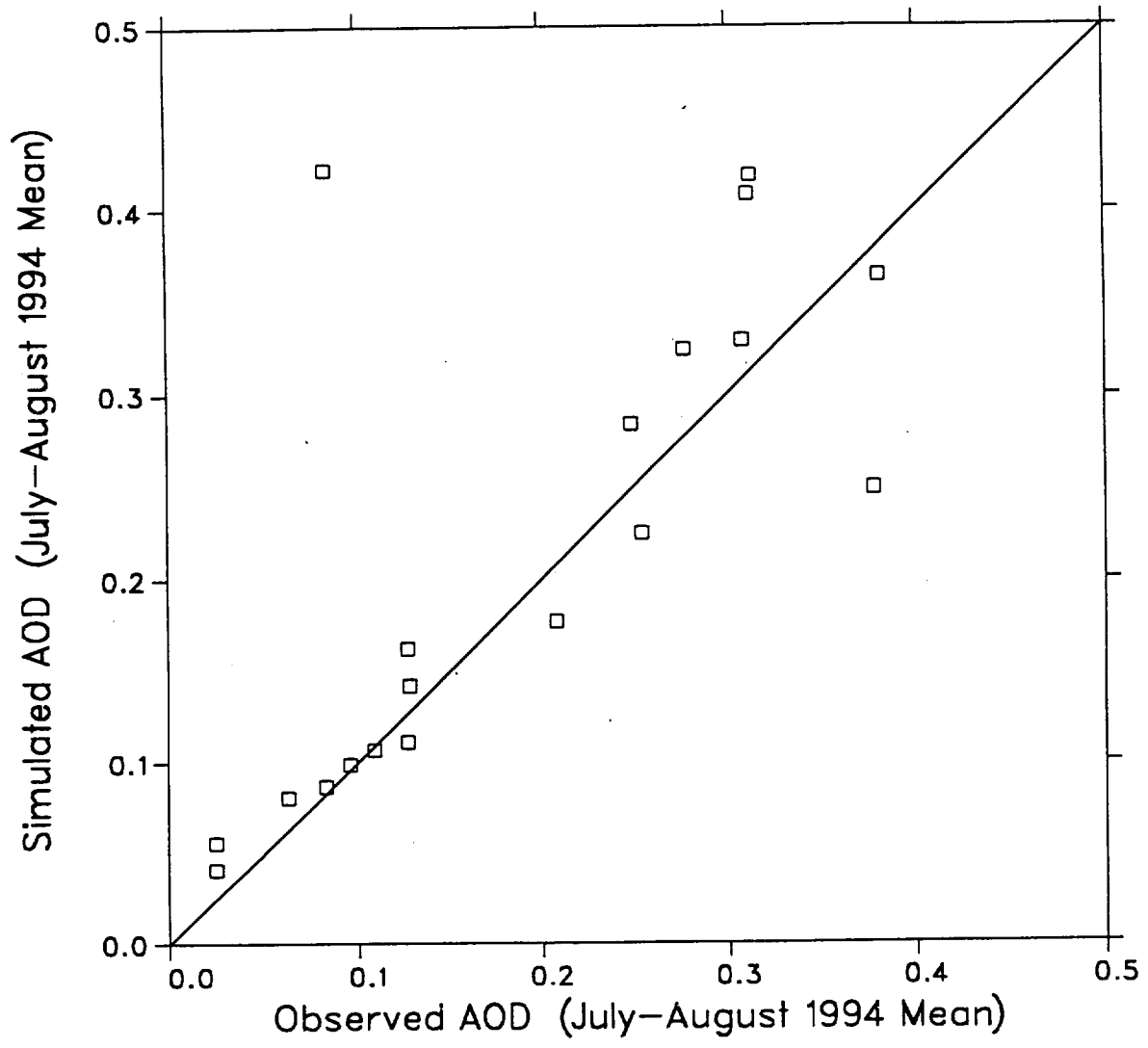


Fig. 4

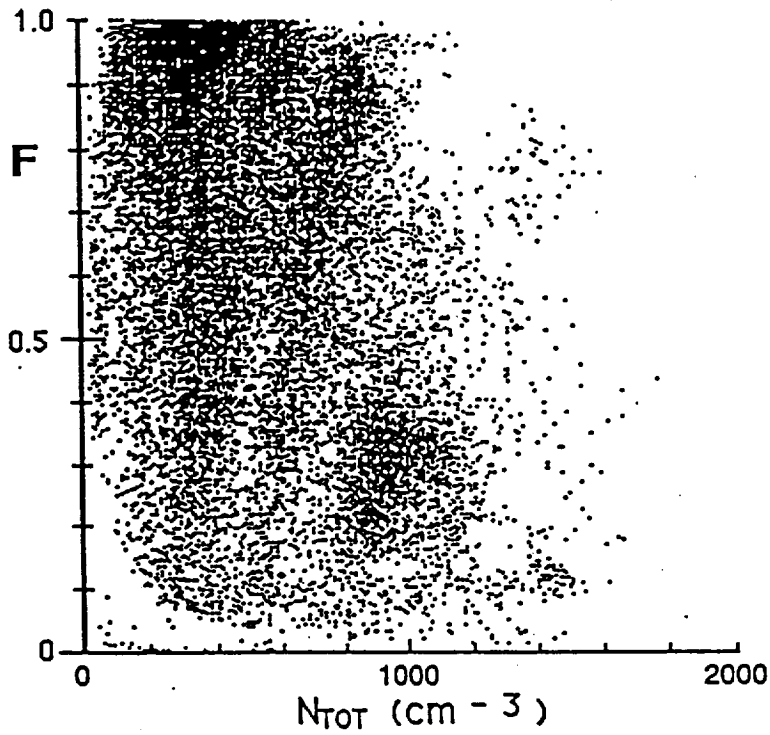


FIGURE 1. F - Data of the Twin Otter for all 10 Days
 (~23200 points)

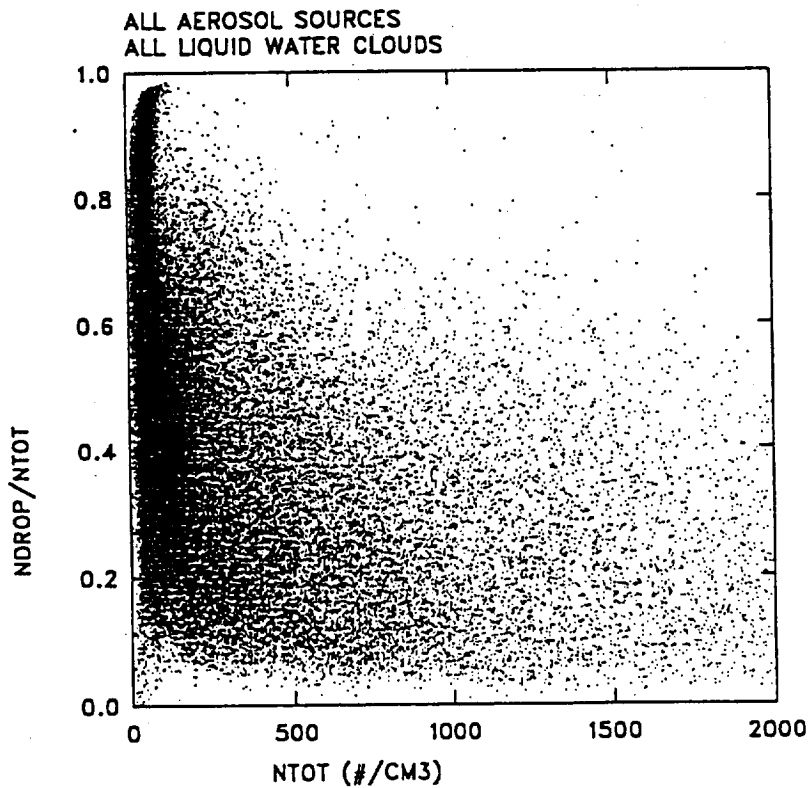


Fig. 5

% OF SAMPLES WITH INDICATED CONCENTRATION

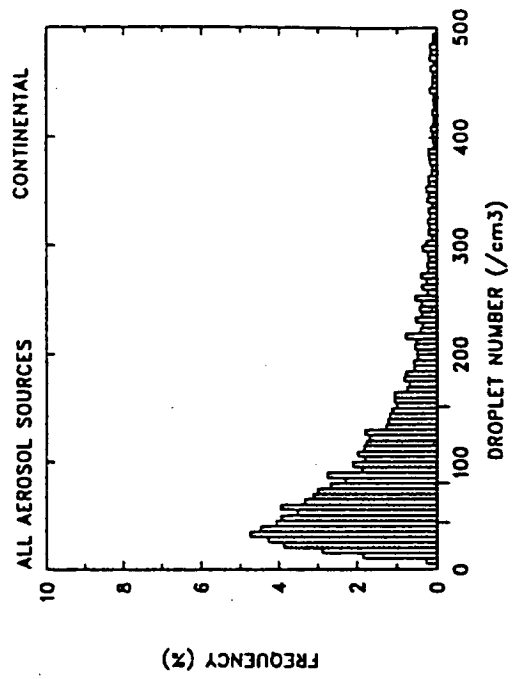
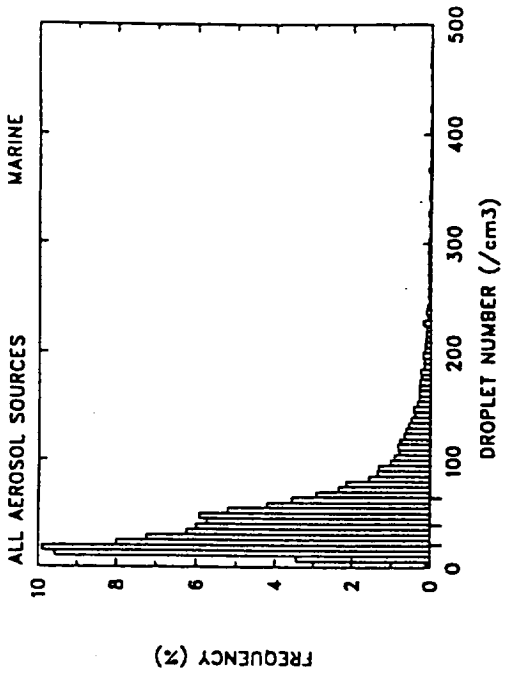
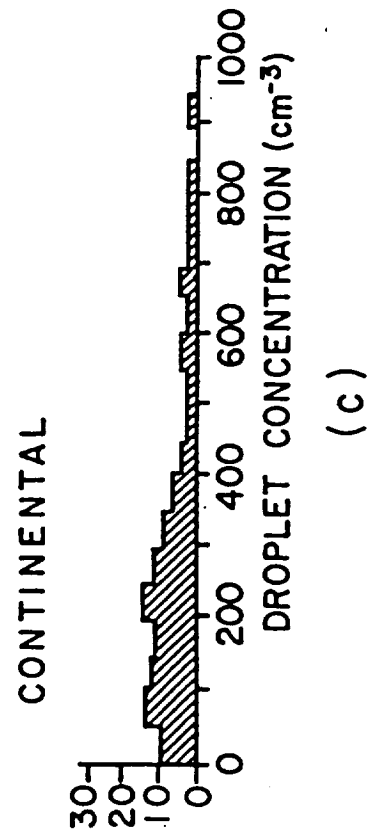


Fig. 6

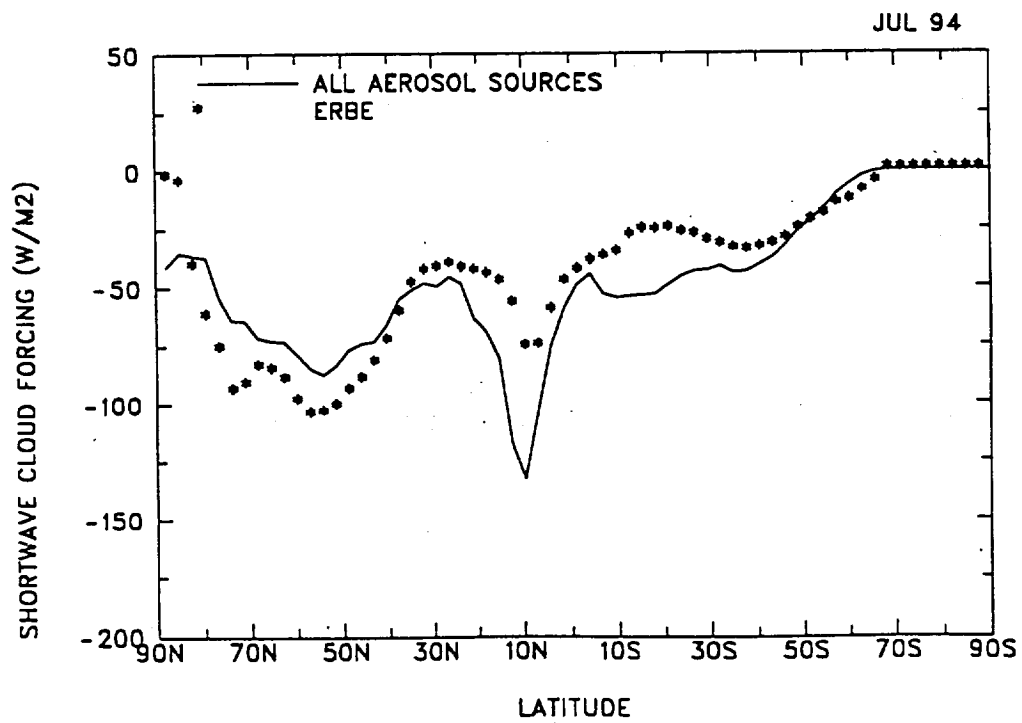
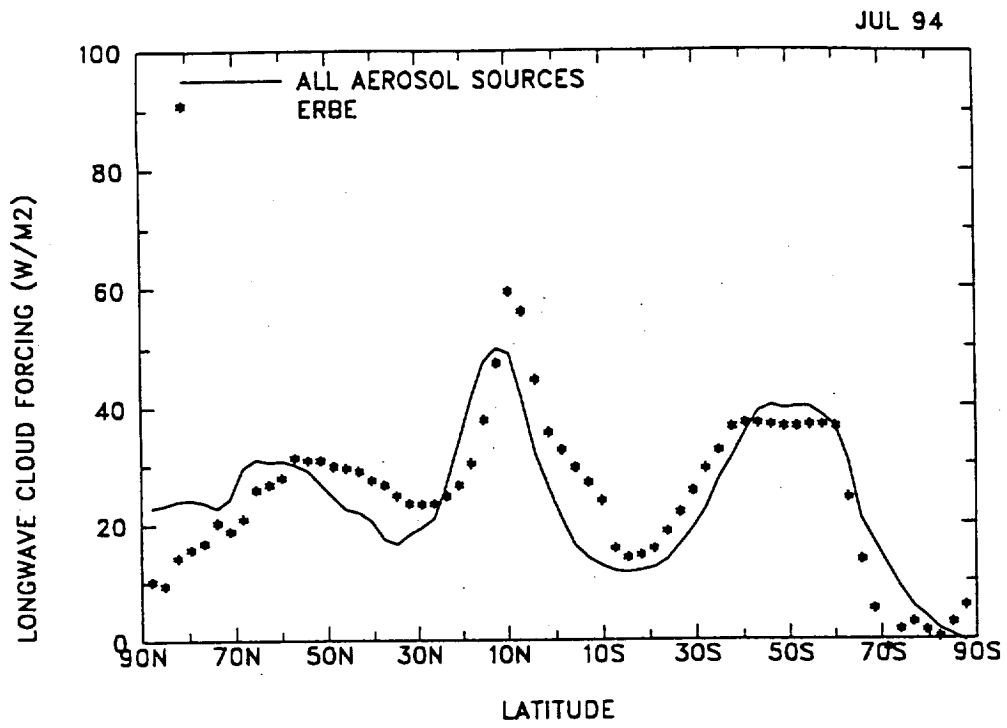


Fig. 7

JUL 94

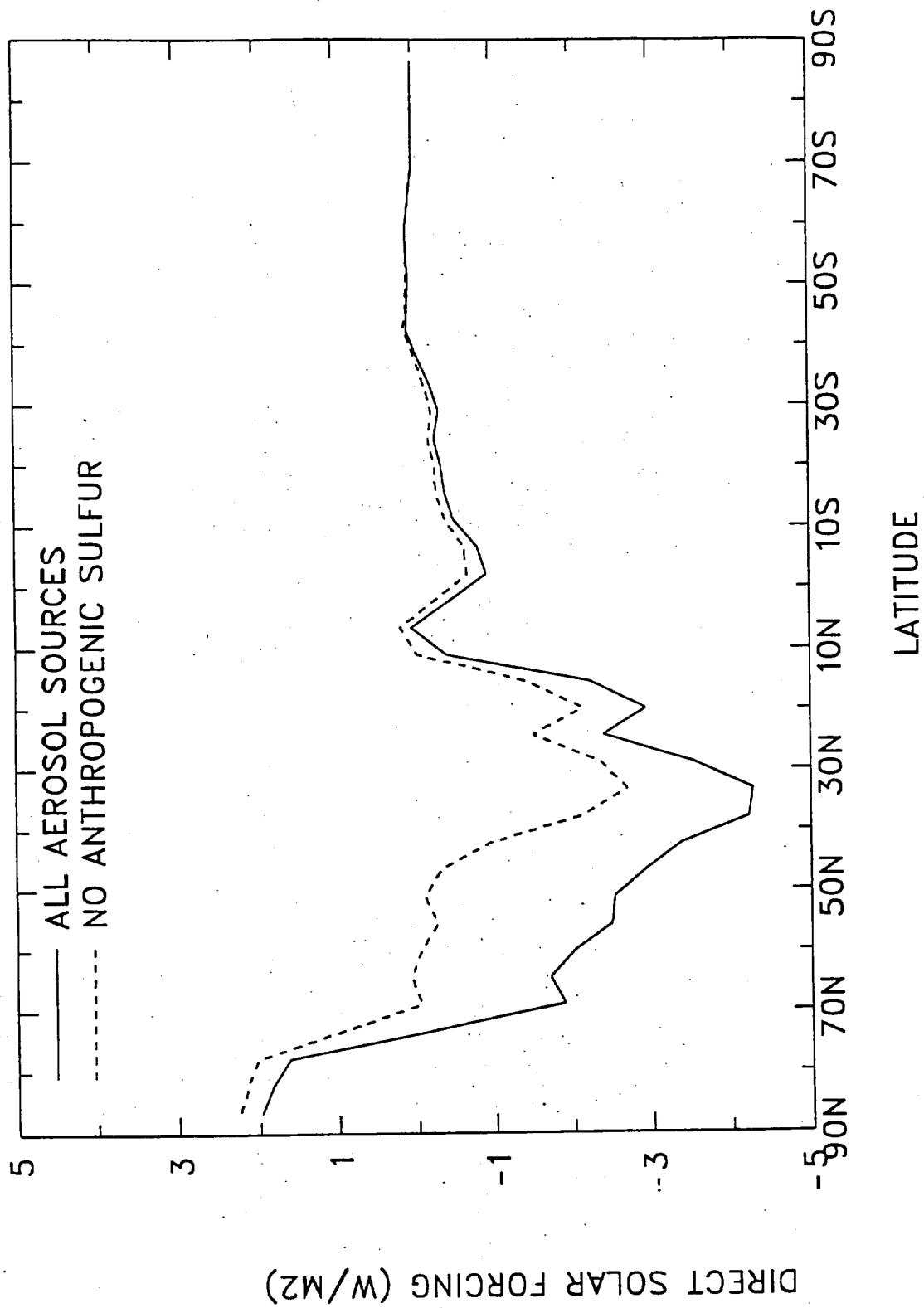


Fig. 8

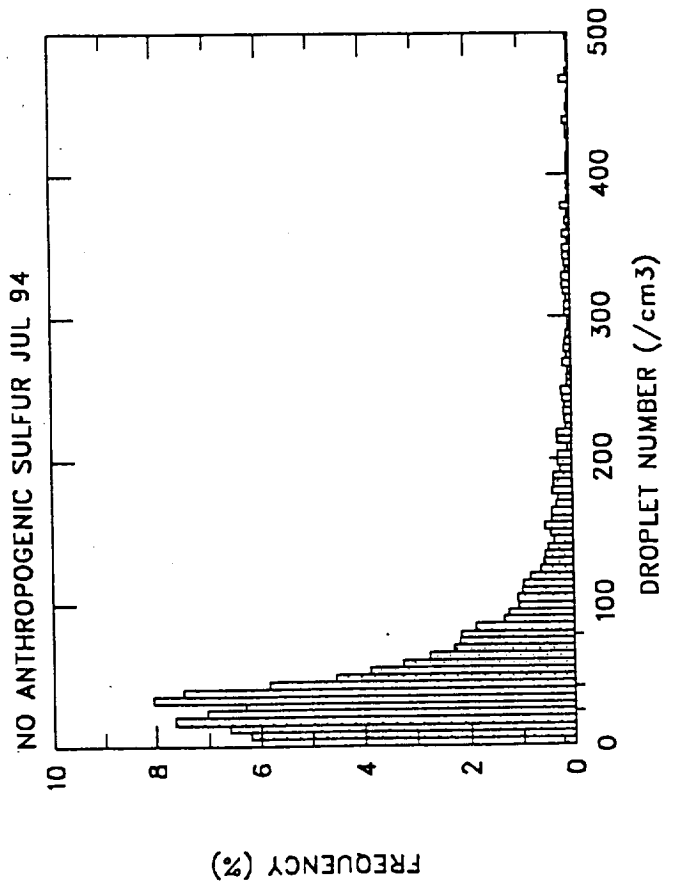
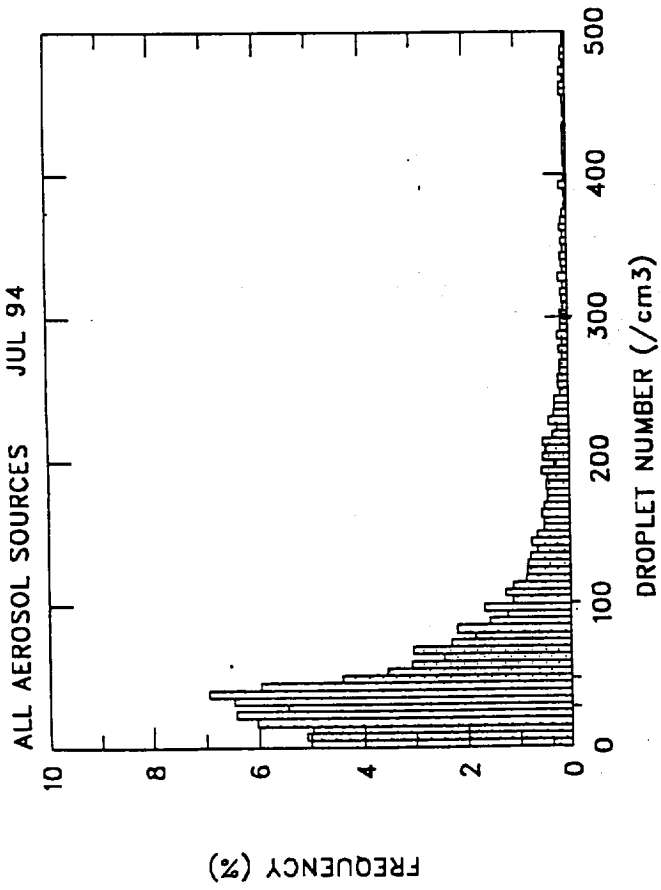


Fig. 9